

## Computational Analysis of Backwards Facing Vortex Generators for Boundary Layer Mixing Applications

K. J. Forster<sup>1</sup>, S. Diasinos<sup>2</sup>, T. J. Barber<sup>1</sup> and G. Doig<sup>1,3</sup>,

<sup>1</sup>School of Mechanical and Manufacturing Engineering  
UNSW Australia, NSW, 2052, Australia

<sup>2</sup>Department of Engineering  
Macquarie University, North Ryde, NSW, 2109, Australia

<sup>3</sup>Aerospace Engineering Department  
California Polytechnic State University, CA 93407, USA

### Abstract

Computational Fluid Dynamics simulations have been performed using RANS and URANS in order to observe the fundamental flow features and differences between various ramp vortex generator geometries. Both forwards and backwards generator geometries have been tested in 3 configurations. From the analysis it was found that the backwards facing ramp produced superior flow entrainment to the near wall region to the forwards facing ramp in a relatively thick boundary layer. A new method for the rapid visualisation of vortex cores has also been proposed.

### Introduction

In order to delay unwanted flow separation from aerodynamic surfaces, a variety of vortex generation techniques are often used to promote boundary layer mixing. Currently the dominant passive vortex generator types used for boundary mixing applications are vane and forward facing ramp generators [5, 6]. However, the lesser-studied backwards facing ramp type generator has shown potential for effective vortex generation in experimental work [1]. This generator type, sometimes used for film cooling applications, produces a counter-rotating vortex pair with a central downwash, as opposed to the central upwash and upwards vortex migration produced by the forward facing ramp type, similar to a delta wing. This effect potentially lengthens the vortex attachment region and delays bursting, depending on the specifics of the generator geometry and resultant lateral vortex migration.

This paper discusses the flow characteristics of both forwards and backwards facing ramp-type vortex generators in three different widths. For ease of comparison to experimental data [1] a length of 36mm (L) and height of 14.5mm were chosen, with widths of 20mm, 30mm and 40mm (0.56L, 0.83L and 1.11L). The approximate geometry of the generators can be seen below in figure 1.

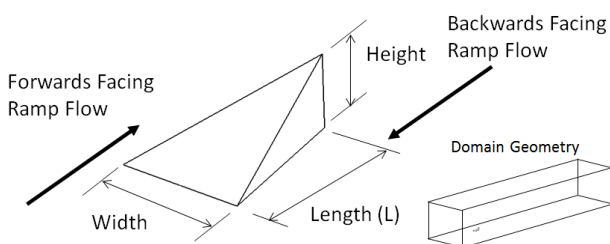


Figure 1. Diagram of vortex generator geometries.

### Numerical Method

To facilitate the rapid evaluation of multiple geometries, RANS second order methods were used for all numerical evaluations, in conjunction with a SIMPLEC algorithm. Grid generation was performed in ANSYS ICEM, with ANSYS FLUENT 14.5 being used to evaluate the model. A fully structured multi-block meshing strategy was employed. To ensure the effectiveness of the mesh in resolving the boundary layer, the  $y^+$  value was kept below 1 on the boundary dominated shear areas, and below 4 in the sharp angled edge regions of the generator where significant separation was expected to occur. The final mesh utilised 150 nodes along the generator length and 56 nodes along the height. It was found that while further increasing the mesh in the wake region from 12 million elements did not noticeably vary the lift and drag coefficients of the vortex generator. The apparent near field flow patterns were also not affected, however the far field vortical structures were considerably altered. Increasing the wake resolution prolonged the length of the low Q-Criterion [4] features, as was to be expected by the reduced diffusion levels in the RANS models from improved mesh resolution. As such the finest resolution mesh available to run within a reasonable timeframe was desired, as any improvement in mesh cell count would yield an improvement in results. This was deemed to be a mesh of approximately 26 million elements, which took around 1 month to run 5000 timesteps on a 64 core 2.1GHz node.

In order to ensure successful comparison to the detailed experimental data of Zaman et. al. [1], a Reynolds number of 20000 based on vortex generator length was selected for all cases. Symmetry boundaries were applied on the sides and top of the model and a no slip smooth wall on the floor. The outlet was specified at zero pressure with respect to the inlet. As the boundary layer was predefined from the experimental data at the vortex generator location, the inlet profile was adjusted to ensure consistency between the computational and experimental models at the generator. This gave a 99% boundary layer thickness at the vortex generator of 0.44L. Variances in outlet length were found to produce negligible differences in vortex generator drag of approximately 0.07%, however differences were observed in the dissipation of vortical properties in the near vortex region, as well as variances in approximate vortex trajectories. To compare these values, streamlines were taken from peak Q-criterion regions, with property values being measured off these streamlines to provide a simple means of comparison between cases.

Through comparison of 4 outlet lengths of 10L, 18L, 26L and 33L, it was found that there was a notable variation from the 10L and 18L cores to the 33L core of up to 8%, however the 26L closely approximated the 33L path with a maximum deviation of

0.7% at a significantly smaller and less computationally intensive domain size. As such, the 26L length was selected for the outlet spacing. The variance between investigated body force values on all the outlet lengths were found to be very similar with maximum errors of around 0.2%. Consequently, the decision on domain length was reliant upon the tracking of the vortex path, rather than the convergence of lift and drag forces.

Wik and Shaw [3] suggested the best turbulence models for vortex generator analysis are the SST K- $\omega$  model and the Reynolds Stress Model, with the SST model typically being preferred due to reduced computational time with very similar results. However, to ensure fidelity across the tests the K- $\epsilon$  realisable, Standard K- $\omega$ , SST K- $\omega$ , Linear Pressure-Strain RSM and Strain - Omega RSM models were tested. The results of these models were then compared against experimental results obtained by Zaman et. al. [1] to determine which was most appropriate. Of the tested turbulence models, the SST k- $\omega$  and Linear Pressure-Strain RSM models were found to have the closest matches to experimental results. From figure 2 it can be seen that while the SST model is a reasonable match for the near region flowfields, the Linear Pressure-Strain RSM model has better correlation, with a far more circular core region and a more accurate disturbance width. The RSM model also had much better correlation in the far wake regions and was selected for further testing, despite its increased computational time.

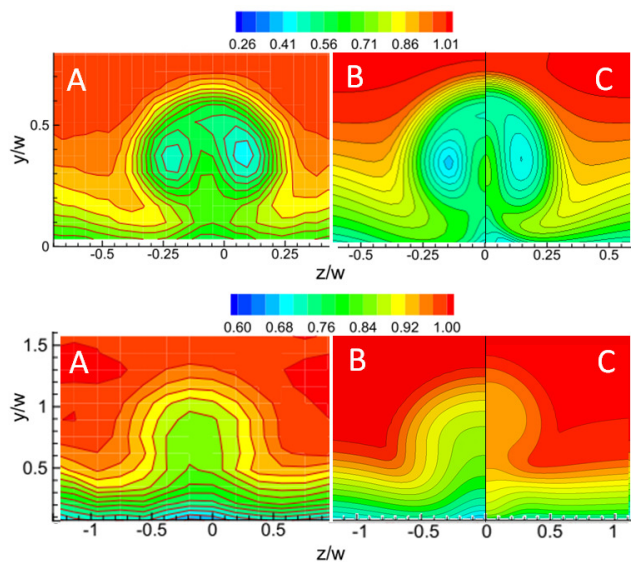


Figure 2. Comparison of data at 1L (top) and 10L (bottom) behind the 0.85L wide forwards facing generator for A) experimental data [1], B) Linear-Strain RSM model and C) SST K- $\omega$  model.

Depending on the geometry and resultant degree of flow separation of the vortex generator, it was possible to run simulations in steady state instead of transient and still achieve convergence. All forward facing geometries as well as the backwards facing 0.56L and 0.83L geometries were able to run successfully in steady state.

### Vortex Tracking Method

Many traditional vortex visualisation methods such as isosurfaces of Q-criterion, Helicity, Vorticity or Lambda-2 [4, 7, 8] rely on flow characteristics which rapidly dissipate as the flow moves away from the geometry. This is a fundamental fluid property which holds true regardless of whether the simulation is RANS, DES or LES. Due to this, an isosurface held at a fixed value for a vortical property will shrink as the vortex progresses. While this accurately describes the reduction of downstream vortex energy, it is not indicative of what is occurring with respect to the vortex

shape, as the core is fundamentally increasing in size and potentially bursting as it travels downstream. In addition to this, there are many special cases where certain criteria do not work at all as identified by Roth [2], such as areas of high boundary shear. As such, a means for accurately tracking the core path and expansion in an easily visualised manner was desired. The commonly used Rankine vortex model combines the flowfield of a potential vortex in the far regions and a solid body rotation in the near core regions to approximate a real world vortex [2]. Observing this model it can be seen that as one progresses away from the vortex centre, the tangential velocity within the vortex plane first increases, then decreases, as per figure 3. This means that any given value of tangential velocity below peak will generate two velocity rings in the plane of the vortex, as indicated by  $r_1$  and  $r_2$  below.

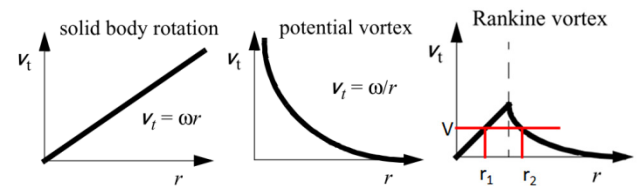


Figure 3. Definition of a Rankine vortex adapted from Roth [2].

Of these two rings, the inner best demonstrates the location of the vortex core and the rate of vortex expansion. The two can be differentiated using a traditional vortex criterion such as the Q-criterion, as the value of the given criterion will be higher near the true centre of the vortex than at the outside. Thus by forming an isosurface at a set tangential velocity, then trimming it using a traditional method, the location of the vortex core can be observed as can be seen in figure 4.

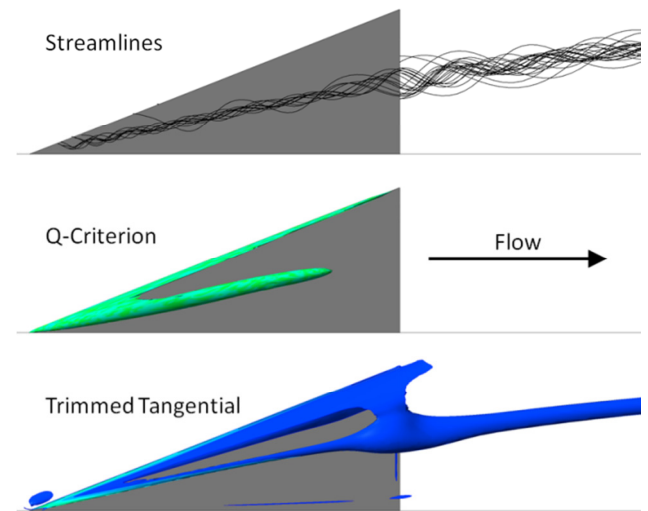


Figure 4. Side view of trimmed tangential velocity isosurface (blue) compared to Q-criterion isosurface (green) and streamlines (black) on 0.56L forwards facing ramp.

In all the cases performed in this study, the tangential velocity isosurface was found to be more accurate than any other criterion at locating and displaying the vortex core, with errors of up to 0.2L in vortex core location at 14L downstream being observed by the Q-Criterion. The error of traditional methods can clearly be seen in figure 5, where the entire first contour of the Q-criterion (where a typical isosurface may be formed) lies entirely outside the clearly observable vortex core.

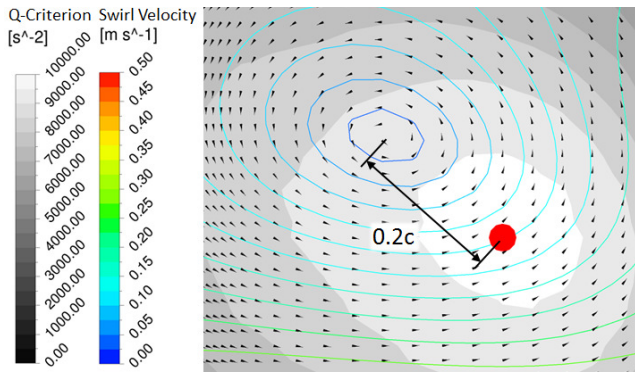


Figure 5. Normalized velocity vectors with contours of tangential velocity (coloured) and contours of Q-criterion (greyscale), with peak indicated in red.

While the method proved successful in the analysis of the vortex generators, there are still a number of limitations to be addressed. As the vortex core progresses downstream, its net swirling velocity is reduced through the transfer of energy to the surrounding flow. This means that this method will visualise the vortex increasing in size at a more rapid rate than it actually is; however will still display a useful surface for tracking the vortex centre. Due to the inherent nature of trying to find a specific tangential velocity from a discrete numerical model, velocity gradients must be used to calculate values and subsequently some artefacts appear such as patchy isosurfaces in near-wall regions and discontinuous surfaces in vortex zones. This is due to the effective radius of the core at a given tangential velocity level shrinking to a cell sized length scale near regions of vortex generation. As such, in order to accurately resolve and track the core throughout the domain, multiple isosurfaces may have to be taken at different tangential velocities and combined in a piecewise fashion.

Currently, the method has been implemented for a flat plate geometry; however this has its own limitations. To locate the true vortex core, the tangential velocity must be found in a plane perpendicular to the direction in which the vortex is travelling. Preliminary investigations into calculating the tangential velocity values on a large number of planes in the approximate direction of vortex travel (as found by points of local peak Q-Criterion) found that the discretisation of the numerical grid resulted in plane directions that were not perfectly aligned with the vortex path. As a result of this the vortex core location would significantly shift from plane to plane due to small deviations in plane angle resulting in large deviations in effective tangential velocity. Consequently it was decided that the most effective way to track the vortex was from the surface of interest (in this case the flat ground plate) rather than the vortex itself. It is proposed that future work could be performed on extending this method to three-dimensionally curved surfaces by producing planes perpendicular to the surface at the point nearest to the location of interest.

## Results

Initial observation of the forces on the generator and the floor of the model indicated that the backwards facing ramps produce substantially more freestream flow entrainment into the near wall region than the forwards facing type, albeit at a higher drag penalty on the generator itself. Figure 6 shows the gains from the different generator geometries over a baseline case, as well as the variances in drag on the generators themselves. An increase of wall shear in this scenario can be thought of as an increase in near wall velocity, which will most likely correlate to superior flow attachment over regions of adverse pressure gradient.

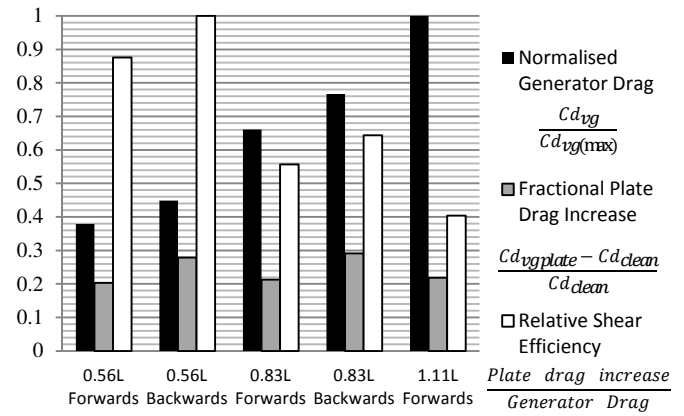


Figure 6. Comparison of force effects of vortex generators.

From this, it can be seen that there is a clear trend to stronger and more effective mixing vortices with the wider generators, as evidenced by the increase in plate drag with increasing vortex generator width. It can also be seen that while the drag penalties are higher for the backwards facing vortex generator types, the efficiencies are notably higher as well.

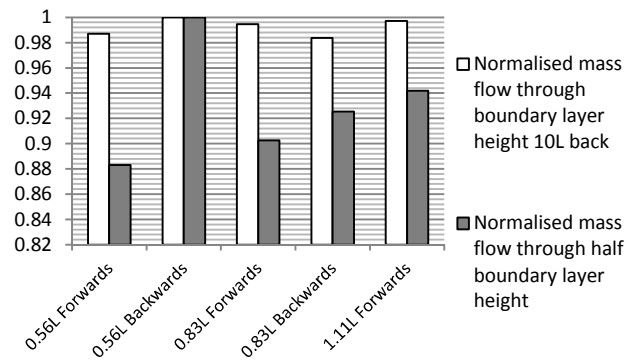


Figure 7. Comparison of mass flows of vortex generators.

Slices were taken horizontally through the half height of the boundary layer after the vortex generator and vertically through the whole height of the boundary layer at a length of 10L downstream from the generator. This was done to determine the mass entrainment of the generator types, as seen in figure 7. These slices were taken through the entire width of the domain to ensure the different generator wake widths were accounted for, and consequently the variations of a few percent seen in figure 7 are actually far more significant in terms of local boundary layer effects. From this, it can be seen that the narrower backwards facing ramp of 0.56L width is the most efficient geometry at entraining flow into the boundary layer, with the forwards facing ramps being notably less efficient. Of note is the decrease in mass entrainment with the wider backwards facing ramp, which is contrary to the shear efficiency from figure 6. This indicates that not only is peak efficiency for a backwards facing ramp achieved at a lower width than a forwards facing generator, but also peak mass entrainment. The discrepancies in the mass flow trends between the horizontal and vertical slices for the forwards ramp indicate that while the average mass flows (horizontal slice) increase with increasing forward ramp width, the mass entrainment effects dissipate at a faster rate (vertical slice, far wake).

Looking at the specifics of the vortex generator flowfields themselves, the reasons behind these differences are revealed. As can be seen in figure 8, the backwards facing ramp generator has a substantially different vortex trajectory to the forwards facing generator, with an initial downwash followed by a steady and

gentle upwards trajectory. This keeps the vortex in much closer proximity to the surface, as well as assisting in the entrainment of high speed, high energy flow into the boundary layer by the generator downwash. The vortex is also generated at a relatively higher point in the boundary layer with more velocity, thus having more initial energy.

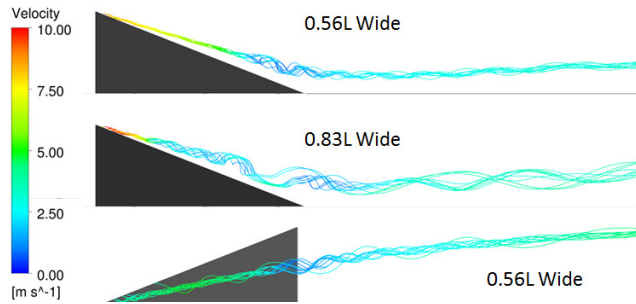


Figure 8. Side view of vortex streamlines from peak Q-criterion isosurface for forwards and backwards ramps.

The difference in vertical displacement can be further seen in the colouring of the streamlines in figure 9, where the forwards facing ramp streamlines continue to increase in height while the backwards ramp streamlines stay close to the surface.

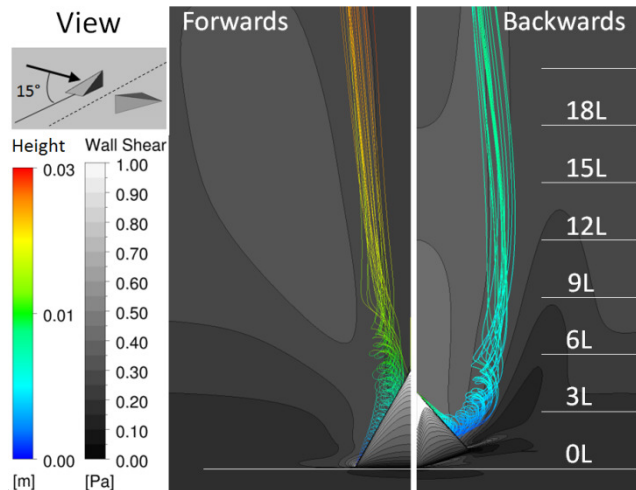


Figure 9. Angled frontal view of vortex streamlines from VG edge coloured by wall height, with contours of wall shear and distance downstream from the vortex generator displayed.

The lateral migration of the vortex core and its resultant shear pattern can also be seen in this figure, with the forwards ramp vortex consistently moving outwards and the backwards ramp vortex initially curving out due to the displacement of the flow by the bow of the generator. The subsequent inwards migration of the core for the backwards case can be explained by the rotation of the vortex shearing against the wall resulting in the vortex being drawn back to the centre. In addition to this, the centrally entrained high speed freestream flow is at a lower pressure, further drawing the vortices inwards. The opposite effect can be seen in the forwards case, where the outwards migration is near constant. Inspecting the near-generator streamlines, it was observed that the different geometry widths resulted in different locations of vortex bursting on the generators themselves, with the adverse pressure gradient clearly increasing with the angle of the side faces. This could explain the efficiency losses observed with the wider generator geometries and can be seen in figure 10. Late and minor bursting is observed on the 0.56L geometry at 0.86L along the surface, whereas on the 0.83L and 1.11L geometries larger scale bursting closer to the leading edge can be seen with a rapid increase in core radius accompanied with a subsequent sharp decrease in velocity. This bursting appears to

be the mechanism by which the vortex increases from a generator relative length scale to a significantly larger length scale.

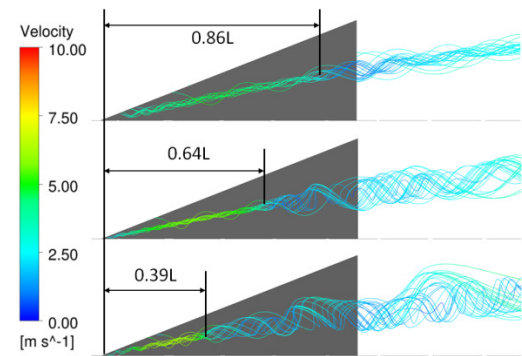


Figure 10. Side view of vortex streamlines from peak Q-criterion isosurface for forwards ramps of 0.56L, 0.83L and 1.11L width.

## Conclusions

The analysis of ramp vortex generators has demonstrated that there may be substantial benefits from using backwards facing ramps in applications where forwards facing ramps are currently used, with a substantial increase in flow entrainment observed. This is particularly evident in areas of thick boundary layers, where the downwash of high velocity flow is especially important. It is anticipated that the superior efficiencies of the backwards facing ramp geometry may diminish in thinner boundary layer conditions. In addition to this, it was found that wider vortex generators produce typically stronger vortices; however this is at the cost of overall vortex efficiency. Future work could be performed on this study using DES and LES. In performing this study, the deficiencies found in traditional vortex visualisation methods were noted and a new method proposed which showed strong initial results.

## References

- [1] Zaman, K., Hirt, S., & Bencic, T. *Boundary Layer Flow Control by an Array of Ramp-Shaped Vortex Generators*, NASA, 2012.
- [2] Roth, M., *Automatic Extraction of Vortex Core Lines and Other Line-Type Features for Scientific Visualization*, ETH Zurich, 2000.
- [3] Wik, E., & Shaw, S. T. *Numerical Simulation of Micro Vortex Generators*. AIAA paper, 2004, 2697.
- [4] J. Jeong and F. Hussain, On the identification of a vortex. *Journal of Fluid Mechanics*, 285, 1995, 69–94.
- [5] Lin, J. C., Review of research on low-profile vortex generators to control boundary-layer separation. *Progress in Aerospace Sciences*, 38, 2002, 389–420.
- [6] Dudek, J. C., Modelling Vortex Generators in a Navier-Stokes Code. *AIAA Journal*, 49, 2011, 748–759.
- [7] Haller, G., An objective definition of a vortex. *Journal of Fluid Mechanics*, 525, 2005, 1–26.
- [8] Theisel, H., Scheuermann, G., & Peikert, R., *Extraction of vortex structures in 3d flow fields*. Edoc.bibliothek.uni-Halle.de, 2009.
- [9] Forster, K., & White, T., Numerical Investigation into Vortex Generators on Heavily Cambered Wings, *AIAA Journal*, 52, 2014, 1059-1071.